Proceedings of the ASME 2023
International Design Engineering Technical Conferences and
Computers and Information in Engineering Conference
IDETC-CIE2023
August 20-23, 2023, Boston, Massachusetts

## DETC2023-116841

# LOCK-IN CONTROL AND MITIGATION OF VORTEX-INDUCED VIBRATIONS IN AIRCRAFT WINGS USING A CONSERVED-MASS NONLINEAR VIBRATION ABSORBER

#### **Ehab Basta**

Department of Mechanical Engineering Virginia Tech, Blacksburg, Virginia 24061

## Sunit K. Gupta

Department of Mechanical Engineering Virginia Tech, Blacksburg, Virginia 24061

## Oumar R. Barry\*

Department of Mechanical Engineering Virginia Tech, Blacksburg, Virginia 24061

## **ABSTRACT**

The impact of the vibration absorber on the synchronization region during vortex-induced vibration of turbine blades is investigated. This work is based on a 3DOF model, including a coupled plunge-pitch airfoil motion and a van der Pol oscillator to the fluid-structure interaction caused by the vortex shedding of the incoming flow. The aeroelastic system is increased by a degree of freedom, namely, the vibration absorber. Linear and nonlinear vibration absorbers are used in this investigation to analyze the effectiveness of the vibration absorber. To demonstrate the effect of the resonator on the lock-in. the coupled natural frequencies, numerical frequency responses, and time histories are plotted. The study reveals the promising capability of the absorber to reduce the lock-in region and mitigate the VIV amplitudes within these regions. For the current application, however, the nonlinear absorber response was indifferent compared to its linear counterpart for the given values of coupling coefficients. This observation indicates that a linear absorber efficiently shrinks the lock-in regions and mitigates the VIV in turbomachinery.

Keywords: Vortex-induced vibration · Passive Vibration absorber · Fluid-structure interaction · Lock-in

### 1. INTRODUCTION

The flow past a circular cylinder, where the fluid flow and vortex shedding produces an aeroelastic phenomenon known as the vortex-induced vibration (VIV), is a well-recognized particular instance of fluid-structure interaction (FSI) that has been closely studied. Vortices alternately separate from each side

of the structure cause VIV [1,2]. Within a certain range of inflow wind speeds, if the vortex shedding frequency is in the vicinity of the structural natural frequency, a phenomenon known as the "lock-in" or "synchronization" occurs [1-4]. High amplitudes are usually observed in the lock-in domain, which inherently exhibits Limit Cycle Oscillation (LCO). Such high amplitude LCO causes high cycle fatigue, undesirable noise, and premature structural failure.

One particular occurrence of VIV is the VIV of an airfoil structure. The airfoil model has numerous applications in the turbomachinery field and has been thoroughly studied by many authors. For instance, Clark et al. [5] showed that an airfoil could exhibit non-synchronous vibrations (NSV)-like behavior in a 2D simulation. This work lays the groundwork for modeling NSV in turbomachinery. Subsequently, many scholars investigated the VIVs of airfoils. Wang et al. [6] constructed a 3DOF model to simulate the VIV of turbine blades. The internal resonance between the turbine blade and the incident flow was studied by formulating a 2DOF airfoil coupled with a VDP oscillator which models the dynamic behavior of the near-wake region. Similarly, Hoskoti et al. [7] incorporated a VDP wake oscillator into a coupled plunge-pitch airfoil and observed the occurrence of the frequency lock-in. The vibrations were predicted analytically, and a parametric study was presented.

Various mitigation techniques have been proposed to overcome the undesirable significant amplitude vibrations due to VIV [8-14]. Within the suppression approaches, a novel active

technique was proposed by Kassem et al. [12] to mitigate flutter using feedback signals from the response of an aeroelastic system. Active control, nevertheless, requires an expensive auxiliary power source for operation. A recently explored suppression option uses an entirely passive, internal, nonlinear energy sink (NES). Interestingly, Blanchard et al. [15] established a rotational NES to suppress a fully turbulent spring cylinder. However, in the case of turbomachinery applications, NES is yet to be shown as more convenient with blunt bodies due to the difficulties in manufacturing and installation. On the other hand, dampers have been applied practically in various research on wind-induced vibrations (WIV). [16-18]

In light of the preceding discussion, to the authors' knowledge, no work has been done on mitigating the onset of the lock-in phenomenon occurring in a coupled plunge-pitch aeroelastic system (airfoil) further coupled with a wake oscillator for fluid modeling. Most previous studies focused on the flutter phenomenon such as in suspension bridges [19] rather than the synchronization onset, which occurs due to the inclusion of the wake oscillator model. In this work, we investigate mitigating the undesirable high amplitudes within the lock-in region of a 3DOF fluid-structure coupled airfoil using a passive linear and a passive nonlinear vibration absorber. The entire mass is conserved, meaning that the absorber's mass is cut from the host structure itself. It is shown in this work that the inclusion of an absorber minimizes the synchronization region and hugely decreases the structural and fluid amplitudes as compared to the previously reported values when the aeroelastic system lacked vibration absorbers. Including a vibration absorber further enables safe flight operations during fluid and structure interaction synchronization. On the other hand, the nonlinearity in the passive absorber is ineffective in reducing the system's vibration during the lock-in.

The rest of the paper is organized as follows. In Section 2, we briefly present the mathematical model for the airfoil along with the von der Pol oscillator to model the fluid-structure interaction. The effect of including the vibration absorber in the lock-in region is explained in Section 3, followed by the effectiveness of the vibration absorber in vibration suppression, detailed in Section 4. Finally, some conclusions are drawn in Section 5.

## 2. MATHEMATICAL MODELING

This section briefly presents the mathematical model for the airfoil structure coupled with the wake oscillator model and the vibration absorber

#### 2.1 The Airfoil Model

The schematic of the conserved-mass aeroelastic system considered in this study is presented in **Fig. 1**. The model's rigid plunging (translation) and pitching (rotation) is

restrained by light, linear springs. A local nonlinear resonator is integrated into the aeroelastic system. Moreover, in this work, the mass of the host structure is conserved by removing the mass equivalent to the additional mass of the absorber. As shown in **Fig. 1**, the absorber, in practice, comprises a cantilever beam with a tip mass equivalent to a mass-spring-damper system. The reference point in the system (where the plunge displacement h is measured) is a point on the elastic axis of the airfoil. Further, the absorber is placed at a distance  $l_1b$  from the elastic axis. The structure can translate vertically (plunge) and rotate (pitch) about the elastic axis. Downward direction is positive plunge motion, and  $\alpha$  is positive when the airfoil is nose up.

The plunge translation, pitch rotation angle, and the absorber's deflection are denoted by h,  $\alpha$  and  $x_1$  respectively. The reader is referred to [6,20] for the detailed discussion of the governing equations of the aeroelastic airfoil structure. Upon the addition of the passive vibration absorber, the three coupled equations governing the plunge, pitch, and absorbers motions are given by

$$m_{T}\ddot{h} + m_{s}bs_{c}\ddot{\alpha} + c_{h}\dot{h} + c_{ab}(\dot{h} - \dot{x}_{1} - l_{1}b\dot{\alpha}) + k_{h1}h + k_{h2}h^{3} + (k_{ab0})(h - x_{1} - l_{1}b\alpha) + (k_{ab2})(h - x_{1} - l_{1}b\alpha)^{3} = -L$$

$$m_{s}bs_{c}\ddot{h} + I_{\alpha}\left(\frac{m_{T}}{m_{s}}\right)\ddot{\alpha} + c_{\alpha}\dot{\alpha} + c_{ab}$$

$$\cdot l_{1}b(\dot{x}_{1} - \dot{h} + l_{1}b\dot{\alpha}) + k_{\alpha1}\alpha + k_{\alpha2}\alpha^{3} + (k_{ab0})l_{1}b(x_{1} - h + l_{1}b\alpha) + (k_{ab2})l_{1}b(x_{1} - h + l_{1}b\alpha)^{3} = M$$

$$(1a)$$

and the equation of the absorber is

$$m_{ab}\ddot{x_1} + c_{ab}(\dot{x_1} - \dot{h} + l_1b\dot{\alpha}) + (k_{ab0})(x_1 - h + l_1b\alpha) + (k_{ab2})(x_1 - h + l_1b\alpha)^3 = 0$$
(1b)

where  $m_T = (m_s + m_f)$ , is the total mass.  $c_h$ ,  $c_\alpha$ , and  $c_{ab}$  are the structural viscous damping coefficients for the plunge, pitch, and absorber motions, respectively.

Introducing the uncoupled natural frequencies of the plunge, pitch, and absorber motions at zero airspeeds, we get

$$\omega_h = \sqrt{\frac{k_{h1}}{m_s}}$$
  $\omega_\alpha = \sqrt{\frac{k_{\alpha 1}}{I_\alpha}}$   $\omega_{ab} = \sqrt{\frac{k_{ab}}{m_{ab}}}$ 

The dimensionless time,  $t^* = \omega_{\alpha}t$ , the dimensionless plunge motion  $h^* = h/b$  and the dimensionless absorber motion  $x_1^* = x_1/b$  are used to non-dimensionalize Eq. (1) to get

$$\lambda \ddot{h} + s_c \ddot{\alpha} + 2\zeta_h \omega_\alpha \dot{h} + 2\zeta_{ab} \omega_b (\dot{h} - \dot{x_1} - l_1 \dot{\alpha}) + \omega_a^2 h$$
$$+ \epsilon_h \omega_a^2 h^3 + \omega_b^2 (h - x_1 - l_1 \alpha)$$
$$+ \epsilon_{ab} \omega_a^2 (h - x_1 - l_1 \alpha)^3 = \tilde{L}$$

$$s_{c}\ddot{h} + \lambda r_{\alpha}^{2} \ddot{\alpha} + 2\zeta_{\alpha}r_{\alpha}^{2} \dot{\alpha} + 2\zeta_{ab}\omega_{b} l_{1} \left(\dot{x}_{1} - \dot{h} + l_{1}\dot{\alpha}\right) + r_{\alpha}^{2} \alpha + \epsilon_{\alpha}r_{\alpha}^{2} \alpha^{3} + \omega_{b}^{2} l_{1} \left(x_{1} - h + l_{1}\alpha\right) + \epsilon_{ab} \omega_{a}^{2} l_{1} \left(x_{1} - h + l_{1}\alpha\right)^{3} = \widetilde{M}$$

$$\mu_{ab}\ddot{x}_{1} + 2\zeta_{ab}\omega_{b} \left(\dot{x}_{1} - \dot{h} + l_{1}\dot{\alpha}\right) + \omega_{b}^{2} \left(x_{1} - h + l_{1}\alpha\right) + \epsilon_{ab} \omega_{a}^{2} \left(x_{1} - h + l_{1}\alpha\right)^{3} = 0$$

$$(2)$$

In the above equations Eq. (2),

$$\lambda = \frac{m_T}{m_S}, \quad \mu_{ab} = \frac{m_{ab}}{m_S}, \quad \omega_a = \frac{\omega_h}{\omega_\alpha}, \quad \omega_b = \frac{\omega_{ab}}{\omega_\alpha},$$

$$\zeta_h = \frac{c_h}{2m_S\omega_h}, \quad \zeta_\alpha = \frac{c_\alpha}{2I_\alpha\omega_\alpha}, \quad \zeta_{ab} = \frac{c_{ab}}{2m_S\omega_{ab}}, \quad (3)$$

$$\epsilon_h = \frac{k_{h2}b^2}{k_{h1}}, \quad \epsilon_\alpha = \frac{k_{\alpha2}}{k_{\alpha1}}, \quad \epsilon_{ab} = \frac{k_{ab2}b^2}{k_{ab0}},$$

$$r_\alpha = \sqrt{\frac{I_\alpha}{m_Sb^2}} \quad \tilde{L} = \frac{-L}{m_Sb\omega_\alpha^2}, \quad \text{and} \quad \tilde{M} = \frac{M}{m_Sb^2\omega_\alpha^2}$$

Note that the ( )\* is dropped from the notation for the sake of simplicity. Here,  $\omega_a$  is the ratio of uncoupled plunge and pitch frequencies and  $\omega_b$  is the ratio of the uncoupled absorber and pitch frequencies;  $\zeta_h$ ,  $\zeta_\alpha$  and  $\zeta_{ab}$  are structural damping coefficients;  $\mu_a$  is the mass ratio;  $\epsilon_h$  and  $\epsilon_\alpha$  are the coefficient of the cubic order nonlinearity of linear and torsional springs, and  $r_\alpha$  is the dimensionless radius of gyration of the section about the elastic axis. For the fluid governing equations, the timevarying aerodynamic lift force and the aerodynamic moment are modeled using the self-excited nonlinear VDP-based wake oscillator.

#### 2.2 The Wake Oscillator

A reduced wake-oscillator model to characterize the oscillating wake uses a generalized dimensionless wake variable q in the VDP equation to represent the vortex-induced timevarying force. The dimensionless governing equations for this model can be expressed as follows:

$$\ddot{q} + \beta f_n (q^2 - 1)\dot{q} + f_n^2 q = f_s \tag{4}$$

where, the coefficient of unsteady vortex lift is expressed by the fluid variable, q. The lift force in terms of the wake variable, q, is given by  $C_L = \frac{1}{2}qC_{L0}$ , where  $C_{L0}$  is the reference lift coefficient of the fluctuating lift force. The angular frequency of the vortex shedding is denoted as  $f_v = 2\pi SV/b$  where S is the Strouhal number, and V is the free stream velocity. Moreover,  $\beta$  is the nonlinear damping coefficient of the wake-oscillator model. The non-dimensionalized representation of Eq. (4) is written as

$$\ddot{q} + \beta \omega_{\nu} (q^2 - 1) \dot{q} + \omega_{\nu}^2 q = F_s \tag{5}$$

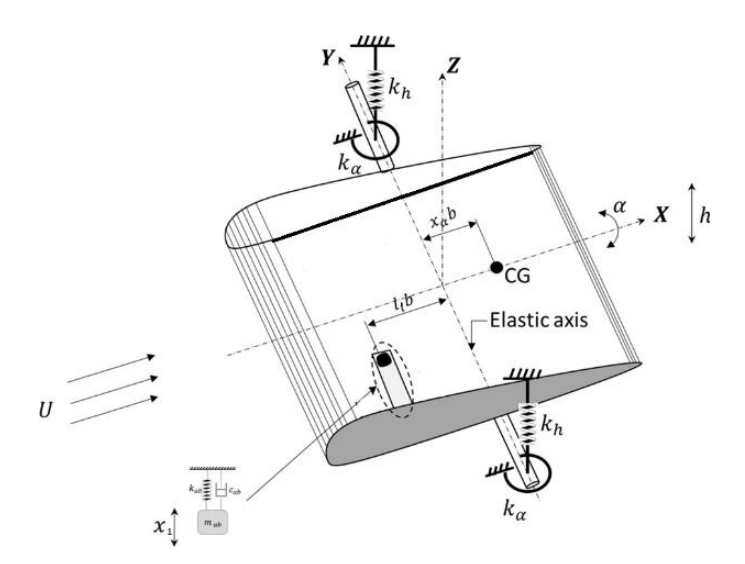


FIGURE 1: FOUR-DEGREE-OF-FREEDOM CROSS-SECTION MODEL OF AN ISOLATED BLADE WITH AN ABSORBER

where  $\omega_v = 2\pi S U_r$  is the dimensionless wake frequency in which  $U_r = V/(b\omega_\alpha)$  is the dimensionless freestream air speed called the reduced velocity. The structural and fluid coupling on the RHS given by  $F_s = f_s/\omega_\alpha^2$  is shown next.

## 2.3 Four DOF Coupled Fluid-Structure Interaction Model

The lift and moment expression, used in the aeroelastic model of the time-varying vortex force resulting from the wake dynamics near the blade, can be written as [20]

$$\tilde{L} = v\omega_v^2 q,$$
  $\tilde{M} = (s_c + 0.5)v\omega_v^2 q$  (6)

where,  $\rho$  is the air density,  $v = \frac{C_{L0}}{8\pi^2 S^2 \mu}$  and  $\mu = \frac{m_s}{\rho b^2}$  are the mass number (to determine the scale of the vortex force on the blade) and the dimensionless mass ratio, respectively. [7]

The forcing term on the structure in the wake-oscillator model in Eq. (6) is assumed to be related to acceleration as

$$F_s = \gamma_1 \ddot{h} + \gamma_2 \ddot{\alpha} + \gamma_3 \ddot{x_1} \tag{7}$$

where  $\gamma_1, \gamma_2$  and  $\gamma_3$  are the coupling coefficients of the wake oscillator corresponding to the plunge, pitch, and absorber motions, respectively. Upon including the motion of the vibration absorber and wake, the coupled 4DOF governing equations read

$$\ddot{h} + s_1 \ddot{\alpha} + \zeta_1 \dot{h} + \zeta_{abh} (\dot{h} - \dot{x}_1 - l_1 \dot{\alpha}) + \omega_1^2 h + \epsilon_1 h^3 + \omega_{bh}^2 (h - x_1 - l_1 \alpha) + \epsilon_3 (h - x_1 - l_1 \alpha)^3 = -\eta_1 \omega_v^2 q$$
 (8)

$$\ddot{\alpha} + s_2 \ddot{h} + \zeta_2 \dot{\alpha} + \zeta_{ab\alpha} l_1 (\dot{x_1} - \dot{h} + l_1 \dot{\alpha}) + \omega_2^2 \alpha + \epsilon_2 \alpha^3 + \omega_{b\alpha}^2 l_1 (x_1 - h + l_1 \alpha) + \epsilon_3 l_1 (x_1 - h + l_1 \alpha)^3 = \eta_2 \omega_v^2 q$$

$$\ddot{q} + \beta \omega_v (q^2 - 1) \dot{q} + \omega_v^2 q = \gamma_1 \ddot{h} + \gamma_2 \ddot{\alpha} + \gamma_3 \ddot{x_1}$$

$$\ddot{x_1} + \zeta_{abx} \left( \dot{x_1} - \dot{h} + l_1 \dot{\alpha} \right) + \omega_{bx}^2 (x_1 - h + l_1 \alpha) + \epsilon_4 (x_1 - h + l_1 \alpha)^3$$

where

$$\zeta_{1} = \frac{2\zeta_{h}\omega_{a}}{\lambda} \qquad \zeta_{2} = \frac{2\zeta_{\alpha}}{\lambda} \qquad \omega_{1}^{2} = \frac{\omega_{a}^{2}}{\lambda} \qquad \omega_{2}^{2} = \frac{1}{\lambda}$$

$$\zeta_{abh} = \frac{2\zeta_{ab}\omega_{b}}{\lambda} \qquad \zeta_{ab\alpha} = \frac{2\zeta_{ab}\omega_{b}}{\lambda r_{\alpha}^{2}} \qquad \zeta_{ab\alpha} = \frac{2\zeta_{ab}\omega_{b}}{\kappa}$$

$$\omega_{bh}^{2} = \frac{\omega_{b}^{2}}{\lambda} \qquad \omega_{b\alpha}^{2} = \frac{\omega_{b}^{2}}{\lambda r_{\alpha}^{2}} \qquad \omega_{bx}^{2} = \frac{\omega_{b}^{2}}{\mu_{ab}} \qquad (9)$$

$$\epsilon_{1} = \frac{\epsilon_{h}\omega_{a}^{2}}{\lambda} \qquad \epsilon_{2} = \frac{\epsilon_{\alpha}}{\lambda} \qquad \epsilon_{3} = \frac{\epsilon_{ab}\omega_{a}^{2}}{\lambda} \qquad \epsilon_{4} = \frac{\epsilon_{ab}\omega_{a}^{2}}{\mu_{ab}}$$

## 3. Lock-in phenomenon

To understand the frequency lock-in phenomenon, the nondimensional linear, un-damped frequencies of the plunge, the pitch, the absorber, and the wake frequencies of the coupled system must be determined. Therefore, the coupled, linear, undamped equations of motion are given by:

 $s_1 = \frac{s_c}{\lambda}$   $s_2 = \frac{s_c}{\lambda r_a^2}$   $\eta_1 = \frac{v}{\lambda}$   $\eta_2 = \frac{v(s + 0.5)}{\lambda r_a^2}$ 

$$\ddot{h} + s_1 \ddot{\alpha} + \omega_1^2 h + \omega_{bh}^2 (h - x_1 - l_1 \alpha) + \eta_1 \omega_v^2 q = 0$$

$$\ddot{\alpha} + s_2 \ddot{h} + \omega_2^2 \alpha + \omega_{b\alpha}^2 l_1 (x_1 - h + l_1 \alpha) - \eta_2 \omega_v^2 q$$

$$= 0$$

$$\ddot{q} + \omega_v^2 q - \gamma_1 \ddot{h} - \gamma_2 \ddot{\alpha} - \gamma_3 \ddot{x_1} = 0$$

$$\ddot{x_1} + \omega_{bx}^2 (x_1 - h + l_1 \alpha) = 0$$
(10)

Assuming the solution of Eq. (10) in the synchronous form as

$$\{h \alpha q x_1\} = \{h_0 \alpha_0 q_0 x_{10}\} e^{i\Omega t}, \tag{11}$$

and substituting into Eq. (10), we obtain the frequency equation. This equation is not reported here for the sake of brevity.

The roots of the frequency equation in ( in terms of  $\Omega^2$ ) are the frequencies of the four DOF-coupled system, i.e.,  $\Omega_i$ , with i=1,2,3 and 4.  $\Omega_1,\Omega_2,\Omega_3$  and  $\Omega_4$  are the dimensionless frequencies of the coupled system, associated with the pitch, plunge, wake-oscillator, and absorber motions, respectively. Further, the occurrence of the internal resonance is determined by the variation of these four natural frequencies of the coupled system with respect to the parameter  $\lambda$ . Unlike the case without absorbers, here,  $\lambda$  is determined as a function of the absorber's

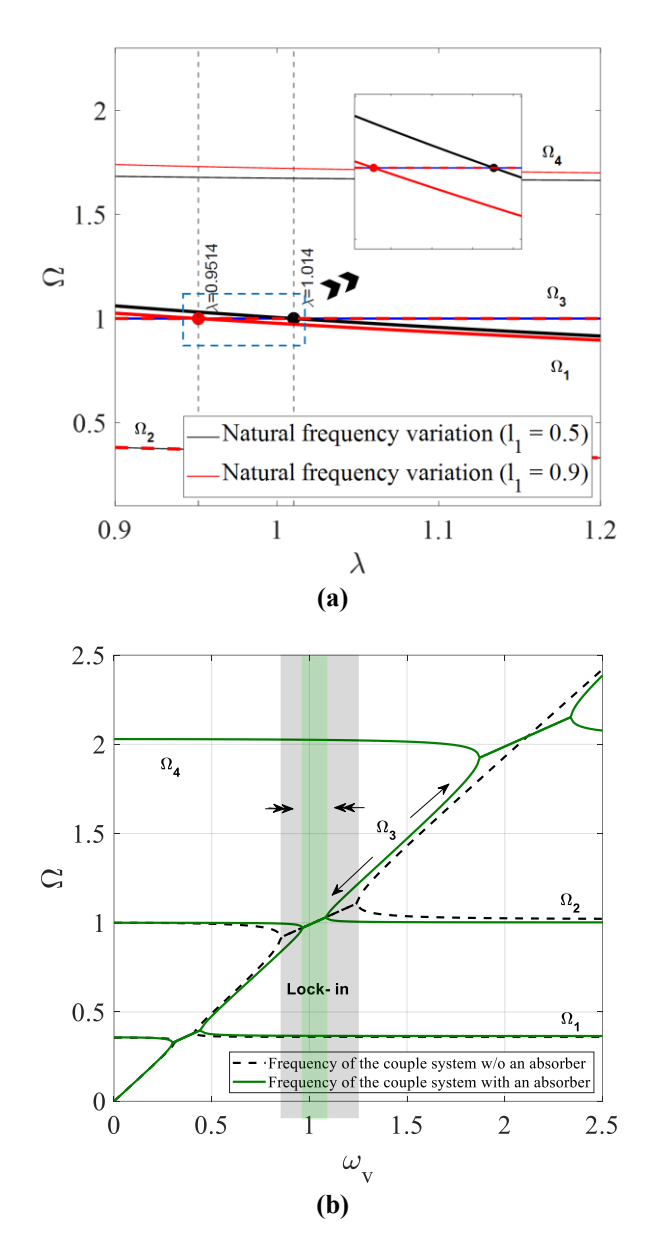


FIGURE 2: a) VARIATION OF THE NATURAL FREQUENCIES WITH THE PARAMETER  $\lambda$  WITH 1: 1 RESONANCE AND b) VARIATION OF THE FREQUENCY OF THE COUPLED SYSTEM WITH RESPECT TO  $\omega_{\nu}$  FOR THE CASES OF WITH AND WITHOUT ABSORBER

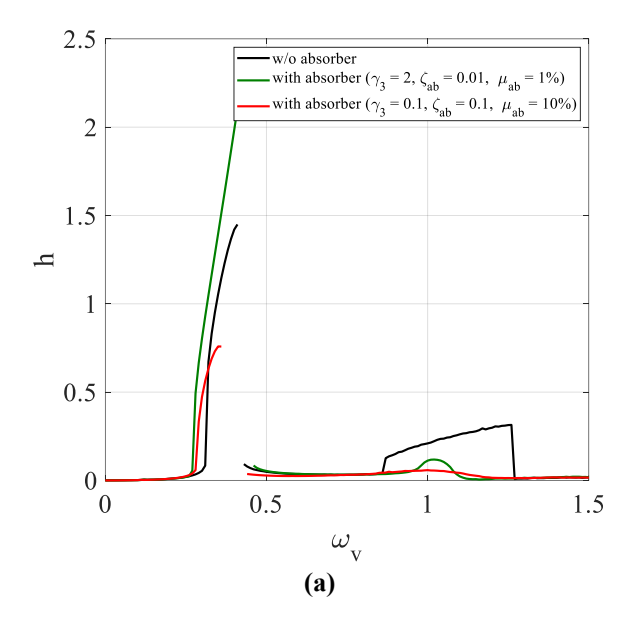
parameters as well as a few others, namely,  $\lambda = f(l_1, \omega_b, s_c, r_\alpha, \omega_\alpha, g_1, g_2, g_3, \mu_\alpha, v)$ . **Fig. 2a** demonstrates the two cases where resonance occurs at  $\lambda = 0.9514$  and  $\lambda = 1.014$  for two different sets of parameters. Herein,  $\lambda$  for any case is a variable calculated by the given parameters. The VDP and structural parameters are fixed for both scenarios in **Fig. 2a**, and they are chosen from the literature [7] where  $\beta = 0.03$ ,  $C_{L0} = 0.2$ ,  $s_c = 0.1, r_\alpha = 0.5$ ;  $\omega_h = 73~Hz, \omega_\alpha = 200Hz$ ,  $\zeta_h = 0.016$ ; and  $\zeta_\alpha = 0.021$ . The absorber's parameters used for each case is (blue)  $l_1 = 0.5, \omega_b = 0.2, \mu_{ab} = 1.5\%$ ,  $\gamma_3 = 2$  and (green)  $l_1 = 0.1, \omega_b = 0.2, \mu_{ab} = 1.5\%$ ,  $\gamma_3 = 2$ .

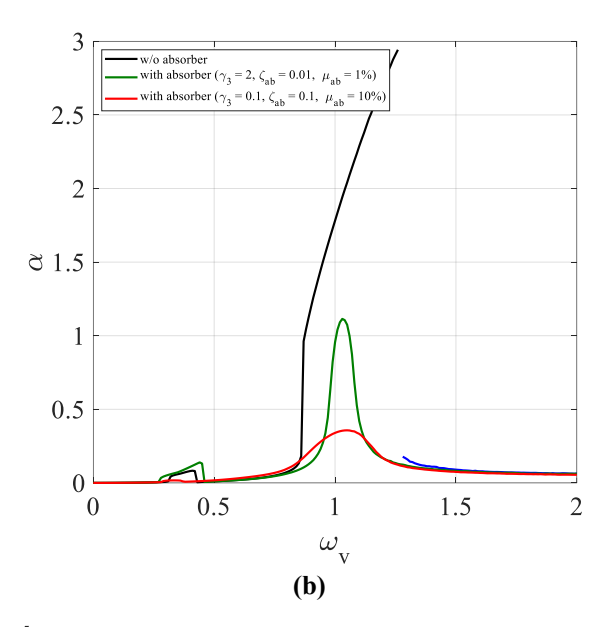
Moreover, the roots of the frequency equation are plotted in **Fig. 2b** as a function of the  $\omega_{\nu}$  with the absorber parameters as  $l_1 = 0.5, \omega_b = 0.2, \mu_{ab} = 1\%, \ \gamma_3 = 2, \text{ hence}, \ \lambda = 1.0252.$  The figure compares the variation for two cases, with and without an absorber [7]. The line  $\Omega = \omega_{\nu}$  corresponds to the wake mode  $\Omega_3$ . The frequency close to unity is the mode associated with the torsional motion  $\Omega_2$ . While the bottom and top frequencies are associated with the plunging and absorber motions, respectively. The figure depicts the impact of the addition of the absorber on the system's lock-in response. In both cases, for certain  $\omega_{\nu}$ values, when the wake mode is near any of the other natural frequencies, the wake mode diverges from the Strouhal law, and the lock-in phenomenon occurs. However, Fig. 2b shows the noticeable minimization of the synchronization region upon adding the absorber. A greater understanding of this figure can be demonstrated using the frequency response curves plotted in Fig. 3.

#### 4. Results and discussion

From figures, Figs. (2b, 3), we can observe that the first lock-in region (viz. bending lock-in) range is unaffected by the incorporation of the absorber. This observation is accompanied by an increase in the amplitude of h and q. At the same time, the response  $\alpha$  is unaffected within this range, as can be seen in **Fig.** 3. For the bending lock-in region with certain parameters, the absorber may show a larger amplitude than the system without the absorbers, as observed in Figs. (3a, 3c). It is also shown, nevertheless, that with few alterations on the absorber parameters, the amplitude during the bending lock-in can be mitigated (red). Next, we focus on the "plunge lock-in," which is shown in Fig. 2b. From Fig. 2b, we can observe the reduction of this plunge lock-in region (green vs. black) upon incorporating the absorber. The same range can be seen in Fig. Figs. (3b,3c), where the lock-in region is reduced along with the mitigated amplitudes of vibrations.

Notice that a third lock-in region in **Fig. 2b** is due to the incorporation of the absorber and is not concerning. However, the plot in **Fig. 4** shows that this third lock-in region occurs for very low damping in the absorber. A slight increase in the absorber's damping almost vanishes this lock-in region, and the amplitudes within this range are highly attenuated.





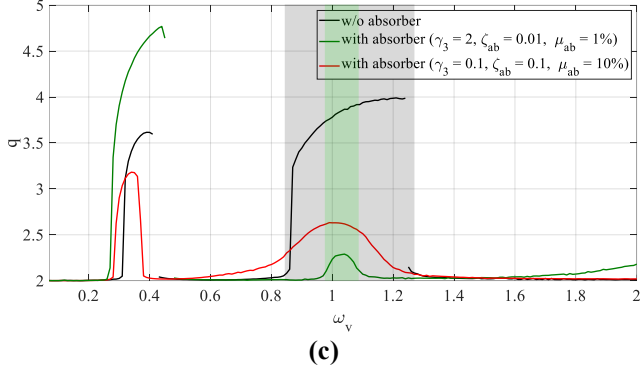


FIGURE 3: FREQUENCY RESPONSES OF THE COUPLED SYSTEM

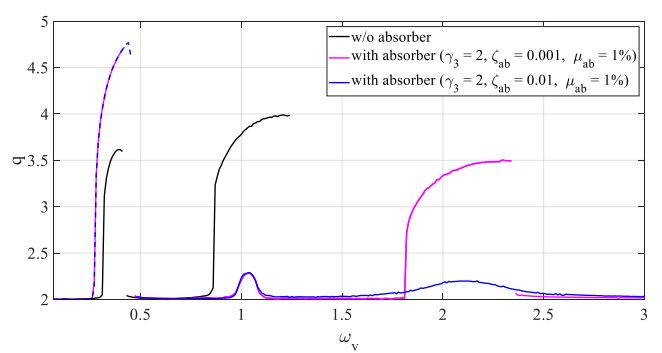
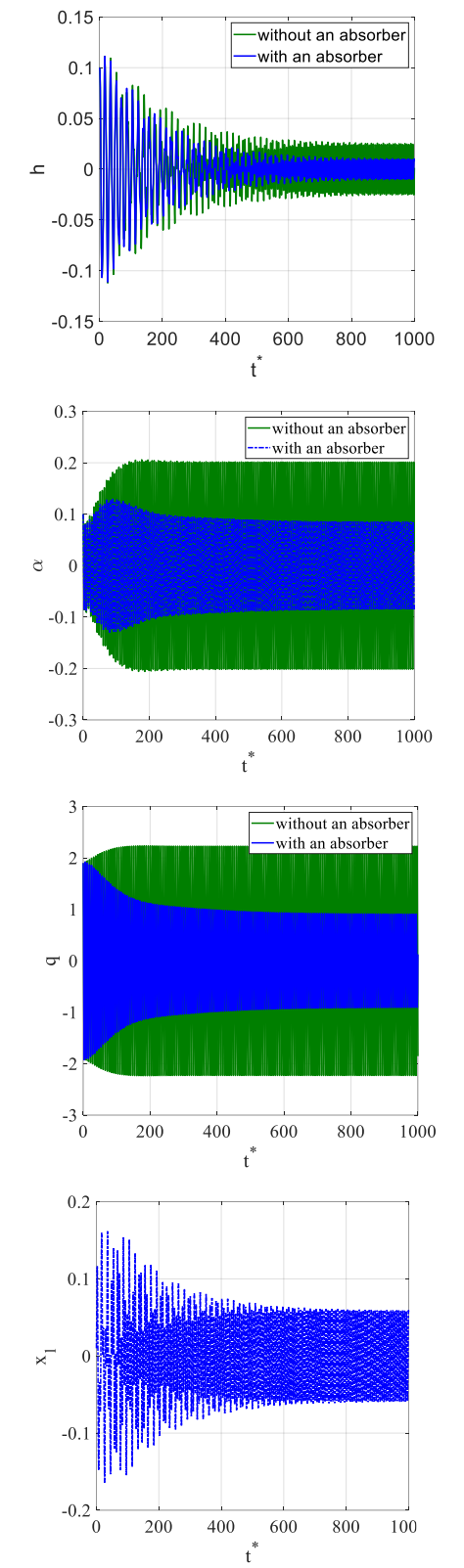


FIGURE 4: FREQUENCY RESPONSE OF THE WAKE-OSCILLATOR FOR DIFFERENT DAMPING RATIOS

To further visualize the absorber's effect on the aeroelastic system's dynamic behavior, time histories of all primary motions of the system are generated at a fixed reduced air stream velocity with and without the vibration absorber. A fourth-order Runge-Kutta method is used to solve the equations to obtain the dynamics response. The absorber values are  $l_1=0.5, \omega_b=0.2, \mu_{ab}=1\%, \ \gamma_3=0.5$  and  $\zeta_{ab}=0.1$ . From Fig. 5, we can observe the VIV mitigation effect of the absorber. The reduction of these amplitudes is explained by the oscillation of the absorber, as seen in Fig. 5d. Here, the absorber oscillates at a relatively higher amplitude. This oscillation is vital in acting as an opposing force to the host structure, and hence the airfoil motion is" absorbed" by the motion of the absorber's mass.

For further numerical investigations, **Fig. 6** compares the frequency responses for the cases of a linear and a nonlinear absorber with two different coupling coefficient values. **Fig.6a** shows that for the current application of interest, and within the same order of magnitude as suggested by the literature [7], the self-excited LCO does not seem to be affected by incorporating a nonlinear absorber as compared to the linear counterpart. This suggests that the forcing within this range of frequencies is not high enough to trigger the nonlinearities in the absorber.

Furthermore, for a theoretical investigation, Fig.6b compares the frequency responses for a higher coupling term, indicating a higher forcing to the system. We observe that the weekly nonlinear absorber spring outperforms its linear absorber counterpart in some instances. However, a highly nonlinear absorber spring degraded the performance compared to the linear absorber spring. This observation further implies that incorporating a nonlinear spring for the absorber may be helpful for certain choices. With the availability of multiple parameters, this becomes more of an optimization problem and is out of the scope of the current study. Moreover, the various parameters affecting the frequency response suggest that analytically predicting the frequency response (e.g., method of multiple scales) will enable us to further understand the effect of certain parameters on the LCO during the synchronization region, which is left for future work.



**FIGURE 5:** COMPARISON OF TIME RESPONSE OF THE SYSTEM

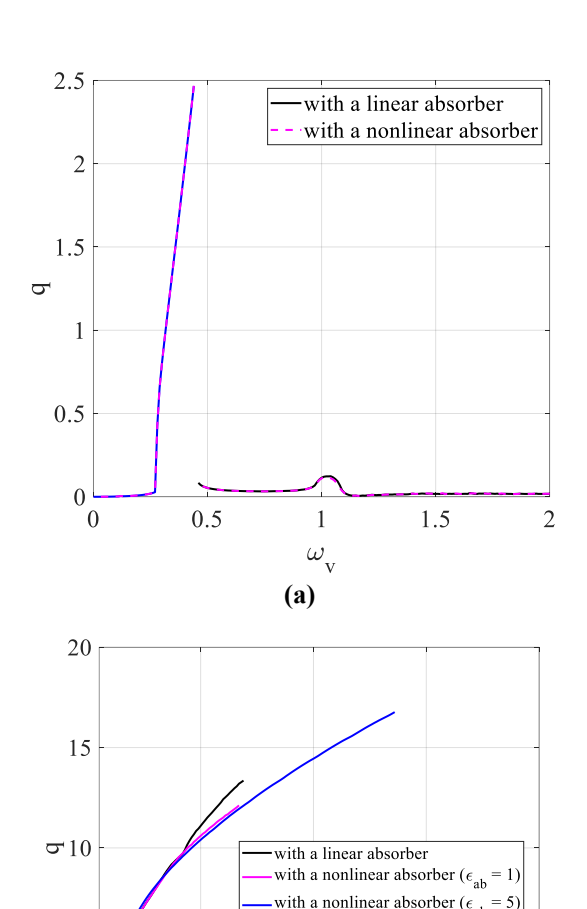


FIGURE 6: EFFECT OF NONLINEARITY IN ABSORBER'S SPRINGS ON THE FREQUENCY RESPONSE FOR (A) LOW COUPLING (B) HIGH COUPLING

**(b)** 

1

 $\omega_{\rm v}$ 

1.5

2

#### 5. CONCLUSION

5

0

0.5

This work investigated the impact of a vibration absorber on the VIV of an airfoil structure subjected to an inflow. Previous studies employed 3DOF governing equations that included the plunge and pitch motion and the VDP as a wake oscillator to represent the interaction between the structure and vortices. Such FSI models elucidated the undesirable phenomenon known as the "lock-in." This FSI model was extended to a four-degree-of-freedom aeroelastic system by incorporating the vibration absorber. Moreover, the entire system was conserved, meaning the absorber's mass was cut from the host structure. This work showed the ability of the vibration absorber to reduce the synchronization region and mitigate the VIV within these regions. This is a promising effect for safer flight operations or turbomachinery applications during the lock-in region speeds.

The reduction in the synchronization region was observed by plotting the coupled system's frequency and the system's corresponding frequency responses with and without the vibration absorber.

Moreover, the time histories at a fixed speed revealed the VIV amplitude mitigation effect of the absorber. Finally, due to the deemed success in literature, the nonlinear absorber was investigated and compared with its linear counterpart. However, the nonlinear absorber did not seem to affect the oscillations within the range of interest. Nevertheless, a higher coupling term showed that a nonlinear absorber might underperform or outperform its linear counterpart, depending on the choice of parameters. The abundance of parameters suggested an optimization study and analytical solutions predict the frequency response to identifying key design parameters for an efficient vibration absorber. These are left for future work.

## **ACKNOWLEDGEMENTS**

This work was funded by (CAREER) - ECCS #1944032: Towards a Self-Powered Autonomous Robot for Intelligent Power Linears Vibration Control and Monitoring

## **REFERENCES**

- [1] C. H. Williamson, "Vortex Dynamics in the cylinder wake," *Annual Review of Fluid Mechanics*, vol. 28, no. 1, pp. 477–539, 1996.
- [2] P. W. Bearman, "Vortex shedding from Oscillating Bluff Bodies," *Annual Review of Fluid Mechanics*, vol. 16, no. 1, pp. 195–222, 1984.
- [3] C. H. K. Williamson and R. Govardhan, "Vortex-induced Vibrations," *Annual Review of Fluid Mechanics*, vol. 36, no. 1, pp. 413–455, 2004.
- [4] R. D. Gabbai and H. Benaroya, "An overview of modeling and experiments of vortex-induced vibration of circular cylinders," *Journal of Sound and Vibration*, vol. 282, no. 3-5, pp. 575–616, 2005.
- [5] S. T. Clark, R. E. Kielb, and K. C. Hall, "A van der pol based reduced-order model for non-synchronous vibration (NSV) in turbomachinery," *Volume 7B: Structures and Dynamics*, 2013.
- [6] D. Wang, Y. Chen, M. Wiercigroch, and Q. Cao, "A three-degree-of-freedom model for vortex-induced vibrations of turbine blades," *Meccanica*, vol. 51, no. 11, pp. 2607–2628, 2016.
- [7] L. Hoskoti, D. A. A., A. Misra, and M. M. Sucheendran, "Frequency lock-in during nonlinear vibration of an airfoil coupled with van der pol oscillator," *Journal of Fluids and Structures*, vol. 92, p. 102776, 2020.

- [8] E. Basta, M. Ghommem, and S. Emam, "Flutter control and mitigation of limit cycle oscillations in aircraft wings using distributed vibration absorbers," *Nonlinear Dynamics*, vol. 106, no. 3, pp. 1975–2003, 2021.
- [9] J. C. Owen, P. W. Bearman, and A. A. Szewczyk, "Passive control of Viv with drag reduction," *Journal of Fluids and Structures*, vol. 15, no. 3-4, pp. 597–605, 2001.
- [10] G. R. S. Assi, P. W. Bearman, N. Kitney, and M. A. Tognarelli, "Suppression of wake-induced vibration of tandem cylinders with free-to-rotate control plates," *Journal of Fluids and Structures*, vol. 26, no. 7-8, pp. 1045–1057, 2010.
- [11] N. Tsushima and W. Su, "Flutter suppression for highly flexible wings using passive and active piezoelectric effects," *Aerospace Science and Technology*, vol. 65, pp. 78–89, 2017.
- [12] M. Kassem, Z. Yang, Y. Gu, W. Wang, and E. Safwat, "Active dynamic vibration absorber for flutter suppression," *Journal of Sound and Vibration*, vol. 469, p. 115110, 2020.
- [13] E. Verstraelen, G. Habib, G. Kerschen, and G. Dimitriadis, "Experimental passive flutter suppression using a linear tuned vibration absorber," *AIAA Journal*, vol. 55, no. 5, pp. 1707–1722, 2017.
- [14] F. Yang, R. Sedaghati, and E. Esmailzadeh, "Vibration suppression of structures using tuned mass damper technology: A state-of-the-art review," *Journal of Vibration and Control*, vol. 28, no. 7-8, pp. 812–836, 2021.
- [15] A. Blanchard, L. A. Bergman, and A. F. Vakakis, "Vortex-induced vibration of a linearly sprung cylinder with an internal rotational nonlinear energy sink in turbulent flow," *Nonlinear Dynamics*, vol. 99, no. 1, pp. 593–609, 2019.
- [16] M. Abdel-Rohman and B. F. Spencer, "Control of windinduced nonlinear oscillations in suspended cables," *Nonlinear Dynamics*, vol. 37, no. 4, pp. 341–355, 2004.
- [17] E. Basta, M. Ghommem, and S. Emam, "Vibration suppression of nonlinear rotating metamaterial beams," Nonlinear Dynamics, vol. 101, no. 1, pp. 311–332, 2020.
- [18] S. K. Gupta, A. L. Malla, and O. R. Barry, "Nonlinear vibration analysis of vortex-induced vibrations in overhead power lines with nonlinear vibration absorbers," Nonlinear Dynamics, vol. 103, no. 1, pp. 27– 47, 2021.

- [19] A. Casalotti, A. Arena, and W. Lacarbonara, "Mitigation of post-flutter oscillations in suspension bridges by hysteretic tuned mass dampers," Engineering Structures, vol. 69, pp. 62–71, 2014.
- [20] D. H. Hodges and G. A. Pierce, *Introduction to structural dynamics and aeroelasticity*. New York, NY: Cambridge University Press, 2014.